



1 **Sensitivity and identifiability of hydraulic and geophysical parameters from**
2 **streaming potential signals in unsaturated porous media**

3

4 Anis Younes^{1,2,3}, Jabran Zaouali¹, Francois Lehmann¹, Marwan Fahs^{*,1}

5 ¹LHyGES, Université de Strasbourg/EOST/ENGEES, CNRS, 1 rue Blessig, 67084 Strasbourg, France.

6 ²IRD UMR LISAH, F-92761 Montpellier, France

7 ³LMHE, ENIT, Tunis, Tunisie

8

9

10 * Contact person: Marwan Fahs

11 E-mail: fahs@unistra.fr



12 **Abstract**

13 Fluid flow in a charged porous medium generates electric potentials called Streaming
14 potential (SP). The SP signal is related to both hydraulic and electrical properties of the soil.

15 In this work, Global Sensitivity Analysis (GSA) and parameter estimation procedures are
16 performed to assess the influence of hydraulic and geophysical parameters on the SP signals
17 and to investigate the identifiability of these parameters from SP measurements. Both
18 procedures are applied to a synthetic column experiment involving a falling head infiltration
19 phase followed by a drainage phase.

20 GSA is used through variance-based sensitivity indices, calculated using sparse Polynomial
21 Chaos Expansion (PCE). To allow high PCE orders, we use an efficient sparse PCE algorithm
22 which selects the best sparse PCE from a given data set using the Kashyap Information
23 Criterion (KIC). Parameter identifiability is performed using two approaches: the Bayesian
24 approach based on the Markov Chain Monte Carlo (MCMC) method and the First-Order
25 Approximation (FOA) approach based on the Levenberg Marquardt algorithm.

26 GSA results show that at short times, the saturated hydraulic conductivity (K_s) and the
27 voltage coupling coefficient at saturation (C_{sat}) are the most influential parameters, whereas,
28 at long times, the residual water content (θ_r), the Mualem-van Genuchten parameter (n) and
29 the Archie's saturation exponent (n_a) become influential with strong interactions between
30 them. The Mualem-van Genuchten parameter (α) has a very weak influence on the SP
31 signals during the whole experiment.

32 Results of parameter estimation show that, although the studied problem is highly nonlinear,
33 when several SP data collected at different altitudes inside the column are used to calibrate the
34 model, all hydraulic (K_s, θ_r, α and n) and geophysical (n_a and C_{sat}) parameters can be
35 reasonably estimated from the SP measurements. Further, in this case, the FOA approach



36 provides accurate estimations of both mean parameter values and uncertainty regions.
37 Conversely, when the number of SP measurements used for the calibration is strongly
38 reduced, the FOA approach yields accurate mean parameter values (in agreement with
39 MCMC results) but inaccurate and even unphysical confidence intervals for parameters with
40 large uncertainty regions.

41

42 **Keywords**

43 Drainage experiment, Streaming Potential, Global Sensitivity Analysis, Markov chain Monte
44 Carlo, parameter estimation.



45 **1. Introduction**

46 Flow through a charged porous medium can generate an electric potential (Zablocki, 1978;
47 Ishido and Mizutani, 1981; Allegre et al., 2010; Jougnot and Linde, 2013), called Streaming
48 Potential (SP). The SP signals play an important role in several applications related to
49 hydrogeology and geothermal reservoir engineering as they are useful for examining
50 subsurface flow dynamics. During the last decade, surface SP anomalies have been widely
51 used to estimate aquifers hydraulic properties (Darnet et al., 2003). Interest on SP is
52 motivated by its low-cost and high sensitivity to water flow. Either coupled or uncoupled
53 approaches can be used for hydraulic parameter estimation from SP signals (Mboh et al.,
54 2012). In the uncoupled approach, Darcy velocities (e.g., Jardani et al., 2007; Bolève et al.,
55 2009) are obtained from tomographic inversion of SP signals and then used for the calibration
56 of the hydrologic model. In the coupled approach, anomalies related to the tomographic
57 inversion are avoided by inverting the full coupled hydrogeophysical model (Hinnell et al.,
58 2010).

59 The SP signals have been widely studied in saturated porous media (Bogoslovsky and Ogilvy,
60 1973; Patella, 1997; Sailhac and Marquis, 2001; Richards et al., 2010; Bolève et al., 2009,
61 among others). Fewer studies focused on the application of the SP signal in unsaturated flow
62 despite the big interest for such nonlinear problems (Linde et al., 2007; Allegre et al., 2010;
63 Mboh et al., 2012; Jougnot and Linde, 2013). Hence, in this work we are interested in the SP
64 signals in unsaturated porous media. Our main objective is to investigate the usefulness of the
65 SP signals for the characterization of soil parameters. To this aim, we evaluate the impact of
66 uncertain hydraulic and geophysical parameters on the SP signals and assess the identifiability
67 of these parameters from the SP measurements.

68 The impact of soil parameters on SP signals is investigated using Global Sensitivity Analysis
69 (GSA). This is a useful tool for characterizing the influential parameters that contribute the



70 most to the variability of model outputs (Saltelli et al., 1999; Sudret, 2008) and for
71 understanding the behavior of the modeled system. GSA has been applied in several areas, as
72 for risk assessment for groundwater pollution (e.g., Volkova et al., 2008), non-reactive
73 (Fajraoui et al., 2011) and reactive transport experiments (Fajraoui et al., 2012; Younes et al.,
74 2016), for unsaturated flow experiments (Younes et al., 2013), natural convection in porous
75 media (Fajraoui et al., 2017) and seawater intrusion (Rajabi et al., 2015; Riva et al., 2015). To
76 the best of our knowledge, GSA has never been used for SP signals in unsaturated porous
77 media. Hence, in the first part of this study, GSA is performed on a conceptual model inspired
78 from the laboratory experiment of Mboh et al. (2012) where SP signals are measured at
79 different altitudes in a sandy soil column during a falling-head infiltration phase followed by a
80 drainage phase. Four uncertain hydraulic parameters (saturated hydraulic conductivity K_s ,
81 residual water content θ_r and fitting Mualem-van Genuchten parameters α and n) and two
82 geophysical (Archie's saturation exponent n_a and voltage coupling coefficient at saturation
83 C_{sat}) parameters are investigated. GSA of SP signals is performed by computing the variance-
84 based sensitivity indices using Polynomial Chaos Expansion (PCE). To reduce the number of
85 PCE coefficients while maintaining high PCE orders, we use the efficient sparse PCE
86 algorithm developed by Shao et al. (2017) which selects the best sparse PCE from a given
87 data set using the Kashyap Information Criterion (KIC).

88 In the second part of this study, we investigate the identifiability of hydro-geophysical
89 parameters from SP measurements. To this aim, parameter estimation is performed using two
90 different approaches. The first approach is a Bayesian approach based on the Markov Chain
91 Monte Carlo (MCMC) method. MCMC has been successfully used in various inverse
92 problems (e.g., Vrugt et al., 2003, 2008; Arora et al., 2012; Younes et al., 2017). The MCMC
93 method yields an ensemble of possible parameter sets that satisfactorily fit the available data.



94 These sets are then employed to estimate the posterior parameter distributions and hence the
95 optimal parameter values and the associated 95% Confidence Intervals (CIs) in order to
96 quantify parameter's uncertainty. The second inversion approach is the commonly used First-
97 Order Approximation (FOA) approach based on the standard Levenberg-Marquardt
98 algorithm. Besides, two scenarios are considered to investigate the effect of lack of data on
99 the parameter identifiability. In the first scenario, SP data collected from sensors at five
100 different locations are taken into account for the calibration. In the second scenario; only the
101 SP data from one sensor are used for model calibration.

102 The present study is decomposed as follows. Section 2 presents the hydrogeophysical model
103 and the reference solution. Section 3 reports on the GSA results of SP signals. Then, Section 4
104 discusses results of parameter estimation with both MCMC and FOA approaches for the two
105 investigated scenarios.

106 **2. Mathematical and conceptual models**

107 **2.1. Mathematical model**

108 The total electrical current density \mathbf{j} [A m^{-2}] is determined from the generalized Ohm's law
109 as follows:

$$110 \quad \mathbf{j} = -\sigma \nabla \varphi + \mathbf{j}_s \quad (1)$$

111 where φ [V] is the streaming potential, \mathbf{j}_s [A m^{-2}] is the streaming current density and σ [S
112 m^{-1}] is the electrical conductivity distribution assumed isotropic.

113 Hence, the conservation equation ($\nabla \cdot \mathbf{j} = 0$) writes

$$114 \quad \nabla \cdot (\sigma \nabla \varphi) = \nabla \cdot \mathbf{j}_s \quad (2)$$

115 Besides, the electrical conductivity distribution can be estimated using the saturation

116 $S_w = \theta / \theta_s$ as follows (Mboh et al., 2012)



117
$$\sigma = \sigma_{sat} S_w^{n_a} \quad (3)$$

118 where σ_{sat} is the electric conductivity at saturation [$S \text{ m}^{-1}$] and n_a is the Archie's saturation
 119 exponent (Archie, 1942).

120 The streaming current density \mathbf{j}_s can be related to the Darcy velocity \mathbf{q} [cm min^{-1}] by (Linde
 121 et al., 2007 ; Revil et al., 2007)

122
$$\mathbf{j}_s = \left(-\sigma_{sat} \frac{\rho g}{K_s} C_{sat} S_w \right) \mathbf{q} \quad (4)$$

123 where K_s is the saturated hydraulic conductivity [cm min^{-1}], ρ is the water density [kg m^{-3}],
 124 g is the gravitational acceleration [m s^{-2}] and C_{sat} is the voltage coupling coefficient at
 125 saturation.

126 Hence, the combination of the previous equations (1-4) leads to the following partial
 127 differential equation governing the SP signals:

128
$$\nabla \cdot (S_w^{n_a} \nabla \varphi) = \nabla \cdot \left(\frac{\rho g C_{sat} S_w}{K_s} \mathbf{q} \right) \quad (5)$$

129 On the other hand, the flow through an unsaturated soil column can be modelled by the one-
 130 dimensional Richard's equation:

131
$$\frac{\partial \theta}{\partial t} = \left(c(h) + S_s \frac{\theta}{\theta_s} \right) \frac{\partial h}{\partial t} = -\nabla \cdot (-K(h) \nabla (h+z)) \quad (6)$$

132 where h [cm] is the pressure head; z [cm] is the depth (downward positive); S_s (-) is the
 133 specific storage; θ_s [$\text{cm}^3 \cdot \text{cm}^{-3}$] and θ are the saturated and actual water contents,
 134 respectively; $c(h)$ [cm^{-1}] is the specific moisture capacity; and $K(h)$ [$\text{L} \cdot \text{T}^{-1}$] is the hydraulic
 135 conductivity. The standard models of Mualem (1976) and Van Genuchten (1980) are used to
 136 relate pressure head, hydraulic conductivity and water content,



$$S_e(h) = \frac{\theta(h) - \theta_r}{\theta_s - \theta_r} = \begin{cases} \frac{1}{(1 + |\alpha h|^n)^m} & h < 0 \\ 1 & h \geq 0 \end{cases} \quad (7)$$

$$K(S_e) = K_s S_e^{1/2} \left[1 - (1 - S_e^{1/m})^m \right]^2$$

137 where S_e (-) is the effective saturation, θ_r [$L^3 \cdot L^{-3}$] is the residual water content, K_s [$cm \cdot min^{-1}$]
 138 is the saturated hydraulic conductivity, $m = 1 - 1/n$, α [cm^{-1}] and n [-] are the Mualem van-
 139 Genuchten shape parameters.
 140

141 2.2. Conceptual model and numerical solution

142 The test case considered in this work is similar to the laboratory experiment developed in
 143 Mboh et al. (2012) involving a falling-head infiltration phase followed by a drainage phase.
 144 This experiment is representative of several laboratory SP experiments (Linde et al., 2007;
 145 Allegre et al., 2010; Jougnot and Linde, 2013, among others). Quartz sand is evenly packed in
 146 a plastic tube with an internal diameter of 5 cm to a height of $L_s = 117.5$ cm. The column is
 147 initially saturated with a ponding of $L_w = 48$ cm above the soil surface. Five sensors allowing
 148 SP measurements are installed at respectively 5, 29, 53, 77, and 101 cm from the surface. The
 149 column has a zero pressure head maintained at its bottom. At the top of the column, the
 150 boundary condition corresponds to a Dirichlet condition with a prescribed pressure head
 151 condition during the falling-head phase followed by a Neumann condition with zero
 152 infiltration flux during the drainage phase. During the falling-head phase, the prescribed
 153 pressure head h_{top} has an exponential behavior driven by the saturated conductivity
 154 $h_{top} = (L_s + L_w) e^{-\frac{K_{st}}{L_s}} - L_s$. The falling-head phase remains until the ponding vanishes at the

155 critical time $t_c = -\frac{L_s}{K_s} \ln\left(\frac{L_s}{L_s + L_w}\right)$.



156 The sandy soil has typical MVG hydraulic parameters with (according to Mboh et al., 2012)
157 $K_s = 29.7$ cm/h, $\theta_s = 0.43$ cm³/cm³, $\theta_r = 0.045$ cm³/cm³, $\alpha = 0.145$ cm⁻¹ and $n = 2.68$. The
158 voltage coupling coefficient at saturation is $C_{sat} = -2.910^{-7}$ V/Pa and the Archie's saturation
159 exponent is $n_a = 1.6$.

160 Based on these hydraulic and geophysical parameters, a reference solution is obtained using a
161 uniform mesh of 235 cells of 0.5 cm length. The system of equations (5)-(6) is solved with the
162 standard finite volume method. The temporal discretization is performed with the method of
163 lines (MOL) which is suitable for strongly nonlinear systems. Indeed, the MOL allows high
164 order temporal integration methods with formal error estimation and control (Miller et al.,
165 1998; Younes et al., 2009; Fahs et al., 2009, 2011).

166 Data are generated from the numerical model by sampling the SP signals every 10 min during
167 1800 min. Figure 1 shows that the SP signals have an almost linear behavior in the saturated
168 falling-head phase. During the drainage phase, they have a nonlinear behavior and approach
169 the zero voltage for the dry conditions occurring toward the end of the experiment. The SP
170 signals are noised with independent Gaussian random noises with a standard deviation of 2.73
171 10^{-5} V. This noise level was obtained by Mboh et al. (2012) from laboratory measurements.
172 The noised data (Fig. 1) are used as "observations" in the calibration exercise.

173 **3. Global sensitivity analysis of SP signals**

174 **3.1. GSA method**

175 The aim of GSA is to assess the effect of the variation of parameters on the model output
176 (Mara and Tarantola, 2008). Such knowledge is important for determining the most influential
177 parameters as well as their regions and periods of influence (Fajraoui et al., 2011). The
178 sensitivity of a model to its parameters can be assessed using Variance-based sensitivity
179 indices. These indices evaluate the contribution of each parameter to the variance of the



180 model (Sobol', 2001). The polynomial chaos theory (Wiener, 1938), has been largely used to
 181 perform variance-based sensitivity analysis of computer models (see for instance, Sudret,
 182 2008; Blatman and Sudret, 2010; Fajraoui et al., 2012; Younes et al., 2016; Shao et al., 2017;
 183 Mara et al., 2017). PCE-based sensitivity analysis is efficient since the Sobol' indices can be
 184 directly obtained from the PCE coefficients without any additional computation (Fajraoui et
 185 al., 2011).

186 Let us consider a mathematical model with a random response $f(\xi)$ which depends on d
 187 independent random parameters $\xi = \{\xi_1, \xi_2, \dots, \xi_d\}$. With PCE, $f(\xi)$ is expanded using a set
 188 of orthonormal multivariate polynomials (up to a polynomial degree p):

$$189 \quad f(\xi) \approx \sum_{|\alpha| \leq p} s_\alpha \Psi_\alpha(\xi) \quad (8)$$

190 where $\alpha = \alpha_1, \dots, \alpha_d \in \mathbb{N}^d$ is a d^{th} -dimensional index. The s_α 's are the polynomial coefficients
 191 and Ψ_α 's are the generalized polynomial chaos of degree $|\alpha| = \sum_{i=1}^d \alpha_i$, such as Hermite,
 192 Legendre and Jacobi polynomials, for instance. In this work, Legendre polynomials are
 193 employed because uniform priors are considered for the parameters.

194 Equation (8) is similar to an ANOVA (Analysis Of Variance) representation of the original
 195 model (Sobol' 1993), from which it is straightforward to express $V[f(\xi)]$, the variance of
 196 $f(\xi)$ as the sum of the partial contribution of the inputs,

$$197 \quad V[f(\xi)] = \sum_{\alpha} s_\alpha^2, \quad (9)$$

198 The first-order sensitivity index S_i and the total sensitivity index ST_i are defined by

$$199 \quad S_i = \frac{V[E[f(\xi)|\xi_i]]}{V[f(\xi)]} \in [0,1], \quad (10)$$



$$ST_i = \frac{E[V[f(\xi)|\xi_i]]}{V[f(\xi)]} \in [0,1], \quad (11)$$

200 where $\xi_{-i} = \xi \setminus \xi_i$, $E[\cdot | \cdot]$ is the conditional expectation operator and $V[\cdot | \cdot]$ the conditional
 201 variance. S_i measures the amount of variance of $f(\xi)$ due to ξ_i alone, while $ST_i \geq S_i$
 202 measures the amount of all contributions of ξ_i to the variance of $f(\xi)$, including its
 203 cooperative non-linear contributions with the other parameters ξ_j . The input/output
 204 relationship is said *additive* when $ST_i = S_i$, $\forall i = 1, \dots, d$, and in this case $\sum_{i=1}^d S_i = 1$.
 205

206 In the sequel, a PCE is constructed for each SP signal at each observable time. The number of
 207 coefficients for a full PCE representation is $P = (d+p)!/(d!p!)$. The evaluation of the PCE
 208 coefficients requires at least P simulations of the nonlinear hydrogeophysical model. Note
 209 that P increases quickly with the order of the PCE and the number of parameters. Hence,
 210 several sparse PCE representations, where only the significant coefficients are sought, have
 211 been proposed in the literature in order to reduce the computational cost of the estimation of
 212 the Sobol indices. For instance, Blatman and Sudret (2010) developed a sparse PCE
 213 representation using an iterative forward-backward approach based on non-intrusive
 214 regression. Fajraoui et al., (2012) developed a technique where only the sensitive coefficients
 215 (that affect significantly model variance) are retained in the PCE. Recently, Shao et al.,
 216 (2017), developed an algorithm based on Bayesian Model Averaging (BMA) to select the best
 217 sparse PCE from a given data set using the Kashyap Information Criterion (KIC) (Kashyap,
 218 1982). The main idea of this algorithm is to increase progressively the degree of an initial
 219 PCE and compute the KIC until obtaining a satisfactory representation of model responses.
 220 This algorithm is used hereafter to compute the sensitivity indices of the SP signals.

221

222 **3.2. GSA results**

223 The SP responses are considered for uniformly distributed parameters over the large intervals
224 shown in Table 1. These intervals include the reference values reported in Mboh et al. (2012).

225 The sensitivity indices of the six input parameters ($K_s, \theta_r, \alpha, n, n_a, C_{sat}$) are estimated using an
226 experimental design formed by $N = 2^{12} = 4096$ parameter sets. The order of the sparse PCE is
227 automatically adapted for each observable time and location. For some observable times, the
228 PCE is highly sparse; it reaches a degree of 31 but contains only 112 nonzero coefficients.

229 Figure 2 depicts the temporal distribution of the streaming potential variance, represented by
230 the blue curve, and the relative contribution of the parameters, represented by the shaded area.

231 This figure corresponds to the temporal ANOVA decomposition for the sensor 1 (at 5 cm
232 from the soil surface) and for the sensor 4 (at 77 cm from the soil surface). Interactions
233 between parameters are represented by the blank region between the variance curves and the
234 shaded area. Note that because Dirichlet boundary condition with zero SP is maintained at the
235 outlet boundary, the variance of the SP signal is zero at the bottom and reaches its maximum
236 value near the soil surface. Hence, the variance is higher for the first sensor, located at 5 cm
237 from the soil surface (Figure 2a) than for the sensor 4 located at 77 cm (Figure 2b).

238 The SP signals at different altitudes exhibit similar behavior (Figure 2). In the following, we
239 comment on the results of sensor 1 (Figure 2a). Because K_s varies between 0.1 [cm min^{-1}]
240 and 2 [cm min^{-1}], the saturated falling-head phase remains until the ponding vanishes at

241 $t_c = -\frac{L_s}{K_s} \ln\left(\frac{L_s}{L_s + L_w}\right)$. Depending on the value of K_s (see Table 1), t_c varies between $t_1 = 20$

242 min and $t_2 = 403$ min. Thus, in Figure 2a, we can see that during a first time period ($t \leq t_1$),

243 the SP signal is strongly influenced by the value of the parameter C_{sat} . The first order and

244 total sensitivity indices at $t = 10$ min (Table 2a) confirm that only the saturated parameters K_s



245 and C_{sat} are influential. C_{sat} is about 17 times more influential than K_s . As expected, the
246 remaining parameters have no influence during the first period. The total variance is 0.72 mv
247 and there is no interaction between the two parameters K_s and C_{sat} since $ST_i = S_i$ for both
248 and $\sum_{i=1}^d S_i = 1$.

249 During the second period ($t_1 \leq t \leq t_2$), the flow is either saturated or unsaturated depending on
250 the value of K_s . Figure 2a shows that the variance of the SP signal exhibits its maximum
251 value around 2.4 mv with strong influences of the parameters K_s and C_{sat} and weak
252 interactions between them (small blank region between the variance curve and the shaded
253 area). These results are confirmed by the sensitivity indices calculated at $t = 70$ min and
254 reported in Table 2a for the sensor 1. Both first order and total sensitivity indices indicate that
255 K_s is the most influential parameter. The second influential parameter is C_{sat} which has a
256 total sensitivity index about 12 times less than K_s . The parameter α is irrelevant since its
257 total sensitivity index is 109 times less than K_s and its partial variance is
258 $V_i = S_i \times V_T = 0.01mv$ which is less than the 95% confidence interval associated to the SP
259 measurement ($\pm 0.055mv$). The total variance at $t = 70$ min is calculated to be 2.17 mv and
260 the output/input relationship is close to be additive since $\sum_{i=1}^d S_i = 0.94$ which means that
261 interactions between parameters exist but are not significant.

262 During the third period ($t \geq t_2$), the variance of the SP signal reduces to 0.3 mv (Figure 2a)
263 and significant interactions are observed between parameters (large blank region between the
264 shaded area and the variance curve). Table 2a shows that for $t = 800$ min, which corresponds
265 to dry conditions, the total variance is 0.22. First-order sensitivity indices are very small,
266 except for θ_r . The latter is highly influential since it has a significant first-order sensitivity



267 index ($S_i = 0.27$) and a more significant total- sensitivity index ($ST_i = 0.74$). The parameters
268 C_{sat} and K_s are irrelevant, they have very small first-order and total sensitivity indices.
269 Further, strong interactions are observed between the parameters since the sum of the first-
270 order indices is far from 1 ($\sum_{i=1}^d S_i = 0.47$). The total sensitivity indices are significantly
271 different from first-order sensitivity indices for almost all parameters. For instance, the ratio
272 between these two indices is around 4 for α , 5 for n_a and 7 for n . The total sensitivity index
273 of α remains small (0.065), whereas, significant total sensitivity indices are obtained for n (
274 $ST_i = 0.27$) and n_a ($ST_i = 0.47$) which indicates that these two parameters are influential
275 (although their first order sensitivity indices are small) because of interaction between
276 parameters.

277 Figure 2b shows similar behavior for the sensor 4 located at 77 cm from the soil surface. The
278 results in Table 2b indicate that the total variance observed at $t = 10, 70$ and 800 min are
279 around 8 times less than for the sensor 1. For the first time period, the first and total
280 sensitivity indices are identical to those observed for the sensor 1 since saturated conditions
281 occur inside the whole column and the same effect of K_s and C_{sat} can be observed whatever
282 the location inside the column. For the second time period, the sensitivity indices for sensor 4
283 (Table 2b) are similar to those observed for the sensor 1. However, the results for the third
284 time period show an improvement of the relevance of the parameter α with an increase of
285 both first and total sensitivity indices. Indeed, compared to the results of the sensor1, both
286 first order and total sensitivity indices have tripled. Moreover, the total sensitivity index for α
287 ($ST_i = 0.22$) becomes close to that of n ($ST_i = 0.24$).

288 In summary, the GSA applied to SP signals identifies the influential parameters and their
289 periods of influence and show that



- 290 - the parameter C_{sat} is highly influential during the first time period ($t \leq t_1$) where no
291 interactions are observed between parameters;
- 292 - the parameter K_s is highly influential during the second time period ($t_1 \leq t \leq t_2$) where
293 small interactions occur between parameters;
- 294 - the parameters θ_r , n and n_a are influential during the third time period ($t \geq t_2$) where
295 dry conditions occur. During this period, strong interactions take place between
296 parameters;
- 297 - the parameter α has no influence on the SP signals during the two first periods and
298 presents a very small influence ($S_i = 0.015$ and $ST_i = 0.065$) during the third period
299 on the sensor 1 (near the surface of the column);
- 300 - the relevance of the parameter α improves with the distance from the soil surface,
301 although the total variance diminishes with respect to this distance. The influence of
302 α becomes significant ($ST_i = 0.22$) on the sensor 4 (located at 77 cm from the soil
303 surface) during the third period.

304 **4. Parameter estimation**

305 **4.1. MCMC and FOA approaches**

306 Calibration of computer models is an essential task since some parameters (like the Mualem
307 van-Genuchten shape parameters α and n) cannot be directly measured. In such an exercise,
308 the unknown model parameters are investigated by facing the model responses to the
309 observations. Recently, Mboh et al. (2012) showed that inversion of SP signals can yield
310 accurate estimate of the saturated hydraulic conductivity K_s , the MVG fitting parameters α
311 and n and the Archie's saturation exponent (n_a). Moreover, they showed that the quality of
312 the estimation was comparable to that obtained from the calibration of pressure heads. In their



313 study, Mboh et al. (2012) used the FOA approach with the Shuffled Complex Evolution
314 optimization algorithm SCE-UA (Duan et al., 1993).

315 As important as the determination of the optimal parameter sets are the associated 95%
316 Confidence Intervals (CIs) to quantify uncertainty on the estimated values. The determination
317 of CIs is not straightforward if the observed model responses are highly nonlinear functions of
318 model parameters (Christensen and Cooley, 1999). In the sequel, parameter estimation is
319 performed using two approaches: the popular FOA approach and the Bayesian approach
320 based on the Markov chain Monte Carlo (MCMC) sampler. The MCMC method is model-
321 free since no assumption concerning model linearity is required for its implementation. Many
322 improvements have been proposed in the literature to accelerate the MCMC convergence rate
323 (e.g., Haario et al., 2006; ter Braak and Vrugt, 2008; Dostert et al., 2009, among others). All
324 MCMC samplers rely on the Metropolis-Hasting algorithm (Metropolis et al., 1953; Hastings,
325 1970). It proceeds as follows:



326 i. Choose an initial candidate $\mathbf{x}^0 = (\xi^0, \sigma^0)$ formed by the initial estimate of the
 327 parameter set ξ^0 and the hyperparameter σ^0 and a proposal distribution q that
 328 depends on the previous accepted candidate.

329 ii. A new candidate $\mathbf{x}^i = (\xi^i, \sigma^i)$ is generated from the current one \mathbf{x}^{i-1} with the
 330 generator $q(\mathbf{x}^i | \mathbf{x}^{i-1})$ associated with the transition probability $p(\xi^i | \mathbf{y}_{mes}, \sigma)$.

331 iii. Calculate $p(\xi^i | \mathbf{y}_{mes}, \sigma)$ and compute the ratio $\alpha = \frac{p(\xi^i | \mathbf{y}_{mes}, \sigma) q(\mathbf{x}^i | \mathbf{x}^{i-1})}{p(\xi^{i-1} | \mathbf{y}_{mes}, \sigma) q(\mathbf{x}^{i-1} | \mathbf{x}^i)}$.

332 Additionally, draw a random number $u \in [0, 1]$ from a uniform distribution.

333 iv. If $\alpha \geq u$, then accept the new candidate, otherwise it is rejected.

334 v. Resume from (ii) until the chain $\{\mathbf{x}^0, \dots, \mathbf{x}^k\}$ converges or a prescribed number of
 335 iterations i_{\max} is reached.

336 Recently, Laloy and Vrugt (2012) developed the DREAM_(ZS) MCMC sampler which runs
 337 multiple chains in parallel for a wider and quicker exploration of the parameter space.

338 However, because of the large number of model evaluations required, the MCMC method
 339 remains rarely used compared to the FOA approach. Indeed, with FOA, the CIs are estimated
 340 once by assuming that the Jacobian remains constant within the CIs. This assumption was
 341 found to be reasonably accurate in nonlinear problems by Donaldson and Scnabel (1987).

342 However, recently, several authors stated that parameter interdependences and model
 343 nonlinearities violate this assumption (see for instance, Vrugt and Bouten, 2002; Vurgin et al.
 344 2007; Gallagher and Doherty, 2007; Mertens et al., 2009; Kahl et al., 2015).

345 In the following, both MCMC and FOA approaches are employed for the inversion of the
 346 highly nonlinear hydrogeophysical problem using SP measurements.

347

348 **4.2. Parameter estimation results**

349 Hydrogeophysical parameters are estimated using the DREAM_(ZS) MCMC sampler (Laloy
350 and Vrugt, 2012). Independent uniform distributions are considered for model parameter
351 priors and likelihood hyperparameters (see Table 1). The parameter posterior distribution
352 writes:

$$353 \quad p(\xi / \mathbf{y}_{mes}, \sigma) \propto \sigma^{-N} \exp\left(-\frac{SS(\xi)}{2\sigma^2}\right) \quad (9)$$

354 where $SS(\xi) = \sum_{k=1}^N (y_{mes}^{(k)} - y_{mod}^{(k)}(\xi))^2$ is the sum of the squared differences between the
355 observed $y_{mes}^{(k)}$ and modeled $y_{mod}^{(k)}$ SP signals at time t_k for N total number of SP
356 observations.

357 The DREAM_(ZS) software computes multiple sub-chains in parallel to thoroughly explore the
358 parameter space. Taking the last 25% of individuals (when the chains have converged) yields
359 multiple sets used to estimate the updated parameter distributions and therefore the optimal
360 parameter values and their CIs. In the sequel, the DREAM_(ZS) MCMC sampler is used with 3
361 parallel chains.

362 We assume that the saturated water content has been initially measured with a fair degree of
363 accuracy. However, instead of fixing its value (as in Kool et al. (1987), van Dam et al. (1994),
364 Nützman et al., (1998) among others), we assign to θ_s a Gaussian distribution to take into
365 account associated uncertainty and its effect on the estimation of the rest of parameters. Hence
366 a Gaussian distribution is assigned to θ_s with a mean value of $0.43 \text{ cm}^3 \cdot \text{cm}^{-3}$ and a 95% CI
367 $[0.41 - 0.45] \text{ cm}^3 \cdot \text{cm}^{-3}$. The rest of parameters are uniformly distributed over the ranges
368 reported in Table 1. The standard deviation σ is also considered unknown and is
369 simultaneously estimated with the physical parameters. Two scenarios are considered: in the
370 first scenario, SP data collected from the sensors located at the five locations are taken into



371 account for the calibration. In the second scenario; only the SP data from the first sensor
372 located at 5 cm from the soil surface serve as conditioning information for model calibration.
373 Results of the MCMC sampler are compared to those of FOA approach for both scenarios.

374 **3.1 Scenario 1: Inversion using all SP measurements**

375 Fig. 3 shows the results obtained with MCMC when the SP data of the five sensors are used
376 for the calibration. The "on-diagonal" plots in this figure display the posterior parameter
377 distributions, whereas the "off-diagonal" plots represent the correlations between parameters
378 in the MCMC sample. Fig. 3 shows bell-shaped posterior distributions for all parameters. A
379 strong correlation is observed between θ_r and n_a ($r = 0.98$).

380 From the obtained MCMC sample, it is straightforward to estimate the posterior 95%
381 confidence interval of each parameter. The latter as well as the mean estimate value of each
382 parameter obtained with both MCMC and FOA approaches are reported in Table 3.

383 The results this table show that the parameters are well estimated from the SP measurements
384 since (i) identified mean values are very close to the reference solution, (ii) all confidence
385 intervals include the reference solution and (iii) the confidence intervals are rather narrow.

386 The saturated parameters K_s and C_{sat} are very well estimated (with CIs around 2%) because
387 of data collected during the falling-head phase where only these two parameters are
388 influential.

389 The posterior CI of the parameter θ_s is similar to its prior CI. The parameter α is reasonably
390 well estimated with a CI around 35%. Recall that this parameter had very small first-order and
391 total sensitivity indices for sensor 1 but had more significant sensitivity indices for the sensors
392 away from the soil surface (see results for sensor 4 in Table 2b). The parameter θ_r is
393 estimated with a CI around 90% although it was highly influential for all sensors (for
394 instance, a first-order sensitivity index of 0.27 and a total order of 0.74 for sensor 1). The



395 parameters n and n_a had similar GSA behavior with small first-order sensitivities
396 (respectively 0.038 and 0.094 for sensor 1) and large total sensitivities (respectively 0.266 and
397 0.4715 for sensor 1), however, the inversion shows that the parameter n is well estimated
398 with a CI less than 10% whereas the parameter n_a is less well estimated with a CI around
399 35%. These results suggest that GSA outcomes should be interpreted with caution in the
400 context of parameter estimation since (i) a parameter which is not relevant for the model
401 output in one sensor can be influential for another sensor and (ii) GSA does not presume on
402 the quality of the estimation since two parameters with similar sensitivity indices can have
403 different quality of estimation by the inversion procedure.

404 Further, the results of Table 3 show that FOA and MCMC approaches yield similar mean
405 estimated values. Moreover, very good agreement is observed between FOA and MCMC
406 uncertainty bounds. Concerning the efficiency of the two calibration methods for this
407 scenario, the FOA approach is by far the most efficient method since it requires only 95s of
408 CPU time. The MCMC method was terminated after 15,000 model runs which required
409 14,116s. The convergence was reached at around 10,000 model runs. The last 5,000 runs were
410 used to estimate the statistical measures of the posterior distribution.

411 **3.2 Scenario 2: Inversion using only SP measurements near the surface**

412 In this scenario, the number of measurements used for the calibration is strongly reduced.
413 Only SP measurements from sensor 1 (located at 5 cm below the soil surface) are considered.
414 The results of MCMC are plotted in the Fig. 4. The correlation observed between θ_r and n_a
415 decreases slightly to $r=0.95$. Almost bell-shaped posterior distributions are observed for all
416 parameters except for the parameters θ_r and α .

417 The results obtained with MCMC and FOA approaches depicted in Table 4 show that



- 418 - The FOA approach yields accurate mean estimated values similar to MCMC results
419 for all parameters;
- 420 - The MCMC and FOA mean estimated values are close to the reference solution and to
421 the previous scenario. The maximum difference is observed for θ_r for which the
422 mean estimated value with scenario 2 is 15% greater than for scenario 1
- 423 - The MCMC CIs for the parameters K_S , θ_s , n and C_{sat} are close to the previous
424 scenario. The parameters θ_s and n are well estimated (CIs < 10%) and the
425 parameters K_S and C_{sat} are very well estimated (CIs \leq 5%).
- 426 - Due to the reduction of the number of data used for model calibration in the scenario
427 2, the MCMC CIs for the parameters n_a , α and θ_r are much larger than in the
428 previous scenario. Indeed, compared to scenario1, the CI for n_a and θ_r increases by
429 around 60% whereas the CI of α is 3 times larger than for the scenario 1.
- 430 - The FOA method yields accurate CIs for the parameters θ_s , n , n_a and C_{sat} whereas it
431 overestimates the CIs of θ_r (by 24%), K_S (by 100%) and α (by 427%). Unphysical
432 uncertainty region (including negative values) is obtained for the parameter α
- 433 These results show that the FOA can fail to provide realistic parameter uncertainties and can
434 yield larger CIs than their corresponding nonlinear MCMC counterpart. Indeed, the
435 linearization in the FOA method assumes that the Jacobian remains constant across the CIs.
436 This assumption was quite fulfilled for the first scenario in which a large number of
437 measurements insured small uncertainty regions. However, the assumption is not fulfilled for
438 some parameters of the current scenario because of the large uncertainty regions induced by
439 the reduction of the number of SP measurements.
- 440 Concerning the efficiency of the calibration methods, the FOA required approximately 174s
441 of CPU time, the MCMC required much more runs to reach the convergence than in the



442 previous scenario. Indeed, the sampler was used with 50,000 runs (35,000 runs were
443 necessary to reach the convergence).

444 **4. Conclusions**

445 In this work, a synthetic test case dealing with SP signals during drainage experiment has
446 been studied. The test case is similar to the laboratory experiment developed in Mboh et al.
447 (2012) involving a falling-head infiltration phase followed by a drainage phase. GSA and
448 Bayesian parameter inference have been applied to investigate (i) the influence of hydraulic
449 and geophysical parameters on the SP signals and (ii) the identifiability of hydro-geophysical
450 parameters using only SP measurements. The GSA was performed using variance-based
451 sensitivity indices which allow measuring the contribution of each parameter (alone or by
452 interaction with other parameters) to the output variance. The sensitivity indices have been
453 calculated using a PCE representation of the SP signals. To reduce the number of coefficients
454 and explore PCE with high orders, we used the efficient sparse PCE algorithm developed by
455 Shao et al. (2017) which selects the best sparse PCE from a given data set using the Kashyap
456 Information Criterion (KIC).

457 The GSA applied to SP signals showed that the parameters C_{sat} and K_s are highly influential
458 during the first period corresponding to saturated conditions. The parameters θ_r , n and n_a
459 are influential when dry conditions occur. In such conditions, strong interactions take place
460 between these parameters. The parameter α has a very small influence on the SP signals near
461 the soil surface but its sensitivity increases with depth although the total variance decreases
462 with depth.

463 Parameter estimation has been performed using MCMC and FOA approaches. All hydraulic (
464 K_s , θ_r , α and n) and geophysical (n_a and C_{sat}) parameters can be reasonably estimated in
465 the first scenario when the whole SP data (measured at five different locations) are used as



466 conditioning information for the model calibration. The confrontation with GSA results shows
467 that the latter should be interpreted with caution when used in the context of parameter
468 estimation since (i) a parameter which is not relevant for the model output in one sensor can
469 be influential for another sensor and (ii) GSA does not presume on the quality of the
470 estimation since two parameters with similar sensitivity indices can have different quality of
471 estimation by the inverse procedure (see for instance, parameters n and n_a). Furthermore,
472 although the studied problem is highly nonlinear, the FOA approach provides accurate
473 estimations of both mean parameter values and CIs in the first scenario and is by far much
474 more efficient than the MCMC method.

475 When the number of SP measurements used for the calibration is considerably reduced (lack
476 of data), the MCMC inversion provides larger parameters' uncertainty regions. The FOA
477 approach yields accurate mean parameter values (in agreement with MCMC results) but
478 inaccurate and even unphysical CIs for some parameters with large uncertainty regions.

479



References

Allègre, V., Jouniaux, L., Lehmann, F. and Sailhac, P.: Streaming potential dependence on water-content in Fontainebleau sand, *Geophysical Journal International*, 182(3), 1248–1266, doi:10.1111/j.1365-246X.2010.04716.x, 2010.

Archie, G. E.: The Electrical Resistivity Log as an Aid in Determining Some Reservoir Characteristics, *Transactions of the AIME*, 146(01), 54–62, doi:10.2118/942054-G, 1942.

Arora, B., Mohanty, B. P. and McGuire, J. T.: Uncertainty in dual permeability model parameters for structured soils, *Water Resources Research*, 48(1), doi:10.1029/2011WR010500, 2012.

Blatman, G. and Sudret, B.: Efficient computation of global sensitivity indices using sparse polynomial chaos expansions, *Reliability Engineering & System Safety*, 95(11), 1216–1229, doi:10.1016/j.res.2010.06.015, 2010.

Bolève, A., Revil, A., Janod, F., Mattiuzzo, J.L. and Fry, J.-J.: Preferential fluid flow pathways in embankment dams imaged by self-potential tomography. *Near Surf. Geophys.* 7:447–462. doi:10.3997/1873-0604.2009012, 2009.

Bogoslovsky, V.A. and Ogilvy, A.A.: Deformation of natural electric fields near drainage structures. *Geophys. Prospect.* 21:716–723. doi:10.1111/j.1365-2478.1973.tb00053, 1973.

ter Braak, C. J. F. and Vrugt, J. A.: Differential Evolution Markov Chain with snooker updater and fewer chains, *Statistics and Computing*, 18(4), 435–446, doi:10.1007/s11222-008-9104-9, 2008.

Christensen, S. and Cooley, R. L.: Evaluation of confidence intervals for a steady-state leaky aquifer model, *Advances in Water Resources*, 22(8), 807–817, doi:10.1016/S0309-1708(98)00055-4, 1999.

van Dam, J. C., Stricker, J. N. M. and Droogers, P.: Inverse Method to Determine Soil Hydraulic Functions from Multistep Outflow Experiments, *Soil Science Society of America Journal*, 58(3), 647, doi:10.2136/sssaj1994.03615995005800030002x, 1994.

Darnet, M., Marquis, G. and Sailhac, P.: Estimating aquifer hydraulic properties from the inversion of surface Streaming Potential (SP) anomalies, *Geophysical Research Letters*, 30(13), doi:10.1029/2003GL017631, 2003.

Donaldson, J. R. and Schnabel, R. B.: Computational Experience with Confidence Regions and Confidence Intervals for Nonlinear Least Squares, *Technometrics*, 29(1), 67, doi:10.2307/1269884, 1987.

Dostert, P., Efendiev, Y. and Mohanty, B.: Efficient uncertainty quantification techniques in inverse problems for Richards' equation using coarse-scale simulation models, *Advances in Water Resources*, 32(3), 329–339, doi:10.1016/j.advwatres.2008.11.009, 2009.

Duan, Q. Y., Gupta, V. K. and Sorooshian, S.: Shuffled complex evolution approach for effective and efficient global minimization, *Journal of Optimization Theory and Applications*, 76(3), 501–521, doi:10.1007/BF00939380, 1993.



Fahs, M., Younes, A. and Lehmann, F.: An easy and efficient combination of the Mixed Finite Element Method and the Method of Lines for the resolution of Richards' Equation, *Environmental Modelling & Software*, 24(9), 1122–1126, doi:10.1016/j.envsoft.2009.02.010, 2009.

Fahs, M., Younes, A. and Ackerer, P.: An Efficient Implementation of the Method of Lines for Multicomponent Reactive Transport Equations, *Water, Air, & Soil Pollution*, 215(1–4), 273–283, doi:10.1007/s11270-010-0477-y, 2011.

Fajraoui, N., Ramasomanana, F., Younes, A., Mara, T. A., Ackerer, P. and Guadagnini, A.: Use of global sensitivity analysis and polynomial chaos expansion for interpretation of nonreactive transport experiments in laboratory-scale porous media, *Water Resources Research*, 47(2), doi:10.1029/2010WR009639, 2011.

Fajraoui, N., Mara, T. A., Younes, A. and Bouhlila, R.: Reactive Transport Parameter Estimation and Global Sensitivity Analysis Using Sparse Polynomial Chaos Expansion, *Water, Air, & Soil Pollution*, 223(7), 4183–4197, doi:10.1007/s11270-012-1183-8, 2012.

Fajraoui, N., Fahs, M., Younes, A. and Sudret, B.: Analyzing natural convection in porous enclosure with polynomial chaos expansions: Effect of thermal dispersion, anisotropic permeability and heterogeneity, *International Journal of Heat and Mass Transfer*, 115, 205–224, doi:10.1016/j.ijheatmasstransfer.2017.07.003, 2017.

Gallagher, M. and Doherty, J.: Parameter estimation and uncertainty analysis for a watershed model, *Environmental Modelling & Software*, 22(7), 1000–1020, doi:10.1016/j.envsoft.2006.06.007, 2007.

van Genuchten, M. T.: A Closed-form Equation for Predicting the Hydraulic Conductivity of Unsaturated Soils, *Soil Science Society of America Journal*, 44(5), 892, doi:10.2136/sssaj1980.03615995004400050002x, 1980.

Haario, H., Laine, M., Mira, A. and Saksman, E.: DRAM: Efficient adaptive MCMC, *Statistics and Computing*, 16(4), 339–354, doi:10.1007/s11222-006-9438-0, 2006.

Hastings, W. K.: Monte Carlo Sampling Methods Using Markov Chains and Their Applications, *Biometrika*, 57(1), 97, doi:10.2307/2334940, 1970.

Hinnell, A. C., Ferré, T. P. A., Vrugt, J. A., Huisman, J. A., Moysey, S., Rings, J. and Kowalsky, M. B.: Improved extraction of hydrologic information from geophysical data through coupled hydrogeophysical inversion, *Water Resources Research*, 46(4), doi:10.1029/2008WR007060, 2010.

Ishido, T., and Mizutani, H.: Experimental and theoretical basis of electrokinetic phenomena in rock–water systems and its applications to geophysics. *J. Geophys. Res.* 86:1763–1775. doi:10.1029/JB086iB03p01763, 1981.

Jardani, A., Revil, A., Bolève, A., Crespy, A., Dupont, J.-P., Barrash, W. and Malama, B.: Tomography of the Darcy velocity from self-potential measurements, *Geophysical Research Letters*, 34(24), doi:10.1029/2007GL031907, 2007.

Jougnot, D. and Linde, N.: Self-Potentials in Partially Saturated Media: The Importance of



Explicit Modeling of Electrode Effects, *Vadose Zone Journal*, 12(2), 0, doi:10.2136/vzj2012.0169, 2013.

Kahl, G. M., Sidorenko, Y. and Gottesbüren, B.: Local and global inverse modelling strategies to estimate parameters for pesticide leaching from lysimeter studies: Inverse modelling to estimate pesticide leaching parameters from lysimeter studies, *Pest Management Science*, 71(4), 616–631, doi:10.1002/ps.3914, 2015.

Kayshap, R.L.: Optimal choice of AR and MA parts in autoregressive moving average models, *IEEE Trans. Pattern Anal. Machine Intell.* 4(2), 99-104, 1982.

Kool, J. B., Parker, J. C. and van Genuchten, M. T.: Parameter estimation for unsaturated flow and transport models — A review, *Journal of Hydrology*, 91(3–4), 255–293, doi:10.1016/0022-1694(87)90207-1, 1987.

Laloy, E. and Vrugt, J. A.: High-dimensional posterior exploration of hydrologic models using multiple-try DREAM_(ZS) and high-performance computing, *Water Resources Research*, 48(1), doi:10.1029/2011WR010608, 2012.

Linde, N., Jougnot, D., Revil, A., Matthäi, S. K., Arora, T., Renard, D. and Doussan, C.: Streaming current generation in two-phase flow conditions, *Geophysical Research Letters*, 34(3), doi:10.1029/2006GL028878, 2007.

Mara, T. A. and Tarantola, S.: Application of global sensitivity analysis of model output to building thermal simulations, *Building Simulation*, 1(4), 290–302, doi:10.1007/s12273-008-8129-5, 2008.

Mara, T. A., Belfort, B., Fontaine, V. and Younes, A.: Addressing factors fixing setting from given data: A comparison of different methods, *Environmental Modelling & Software*, 87, 29–38, doi:10.1016/j.envsoft.2016.10.004, 2017.

Mboh, C. M., Huisman, J. A., Zimmermann, E. and Vereecken, H.: Coupled Hydrogeophysical Inversion of Streaming Potential Signals for Unsaturated Soil Hydraulic Properties, *Vadose Zone Journal*, 11(2), 0, doi:10.2136/vzj2011.0115, 2012.

Mertens, J., Kahl, G., Gottesbüren, B. and Vanderborght, J.: Inverse Modeling of Pesticide Leaching in Lysimeters: Local versus Global and Sequential Single-Objective versus Multiobjective Approaches, *Vadose Zone Journal*, 8(3), 793, doi:10.2136/vzj2008.0029, 2009.

Metropolis, N., Rosenbluth, A. W., Rosenbluth, M. N., Teller, A. H. and Teller, E.: Equation of State Calculations by Fast Computing Machines, *The Journal of Chemical Physics*, 21(6), 1087–1092, doi:10.1063/1.1699114, 1953.

Miller, C. T., Williams, G. A., Kelley, C. T. and Tocci, M. D.: Robust solution of Richards' equation for nonuniform porous media, *Water Resources Research*, 34(10), 2599–2610, doi:10.1029/98WR01673, 1998.

Mualem, Y.: A new model for predicting the hydraulic conductivity of unsaturated porous media, *Water Resources Research*, 12(3), 513–522, doi:10.1029/WR012i003p00513, 1976.



Nützmann, G., Thiele, M., Maciejewski, S. and Joswig, K.: Inverse modelling techniques for determining hydraulic properties of coarse-textured porous media by transient outflow methods, *Advances in Water Resources*, 22(3), 273–284, doi:10.1016/S0309-1708(98)00009-8, 1998.

Patella, D.: Introduction to ground surface self-potential tomography. *Geophys. Prospect.* 45:653–681. doi:10.1046/j.1365-2478.1997.430277, 1997.

Rajabi, M. M., Ataie-Ashtiani, B. and Simmons, C. T.: Polynomial chaos expansions for uncertainty propagation and moment independent sensitivity analysis of seawater intrusion simulations, *Journal of Hydrology*, 520, 101–122, doi:10.1016/j.jhydrol.2014.11.020, 2015.

Revil, A., Linde, N., Cerepi, A., Jougnot, D., Matthäi, S. and Finsterle, S.: Electrokinetic coupling in unsaturated porous media, *Journal of Colloid and Interface Science*, 313(1), 315–327, doi:10.1016/j.jcis.2007.03.037, 2007.

Richards, K., Revil, A., Jardani, A., Henderson, F., Batzle, M., and Haas, A.: Pattern of shallow ground water flow at Mount Princeton Hot Springs, Colorado, using geoelectric methods. *J. Volcanol. Geotherm. Res.* 198:217–232. doi:10.1016/j.jvolgeores.2010.09.001, 2010.

Riva, M., Guadagnini, A. and Dell’Oca, A.: Probabilistic assessment of seawater intrusion under multiple sources of uncertainty, *Advances in Water Resources*, 75, 93–104, doi:10.1016/j.advwatres.2014.11.002, 2015.

Sailhac, P. and Marquis, G.: Analytic potentials for the forward and inverse modeling of SP anomalies caused by subsurface fluid flow, *Geophysical Research Letters*, 28(9), 1851–1854, doi:10.1029/2000GL012457, 2001.

Saltelli, A., Tarantola, S. and Chan, K. P.-S.: A Quantitative Model-Independent Method for Global Sensitivity Analysis of Model Output, *Technometrics*, 41, 39–56, doi:10.1080/00401706.1999.10485594, 1999.

Shao, Q., Younes, A., Fahs, M. and Mara, T. A.: Bayesian sparse polynomial chaos expansion for global sensitivity analysis, *Computer Methods in Applied Mechanics and Engineering*, 318, 474–496, doi:10.1016/j.cma.2017.01.033, 2017.

Sobol’, I. .: Global sensitivity indices for nonlinear mathematical models and their Monte Carlo estimates, *Mathematics and Computers in Simulation*, 55(1–3), 271–280, doi:10.1016/S0378-4754(00)00270-6, 2001.

Sobol’, I. M.: Sensitivity estimates for nonlinear mathematical models, *Math. Model. Comput. Exp.*, 407–414, 1993.

Sudret, B.: Global sensitivity analysis using polynomial chaos expansions, *Reliability Engineering & System Safety*, 93(7), 964–979, doi:10.1016/j.res.2007.04.002, 2008.

Volkova, E., Iooss, B. and Van Dorpe, F.: Global sensitivity analysis for a numerical model of radionuclide migration from the RRC “Kurchatov Institute” radwaste disposal site, *Stochastic Environmental Research and Risk Assessment*, 22(1), 17–31, doi:10.1007/s00477-006-0093-y, 2008.



Vrugt, J., Gupta, H. V., Bouten, W. and Sorooshian, S.: A Shuffled Complex Evolution Metropolis algorithm for optimization and uncertainty assessment of hydrologic parameter estimation, *Water Resour. Res.*, 39, 2003.

Vrugt, J. A. and Bouten, W.: Validity of First-Order Approximations to Describe Parameter Uncertainty in Soil Hydrologic Models, *Soil Science Society of America Journal*, 66(6), 1740, doi:10.2136/sssaj2002.1740, 2002.

Vrugt, J. A., ter Braak, C. J. F., Clark, M. P., Hyman, J. M. and Robinson, B. A.: Treatment of input uncertainty in hydrologic modeling: Doing hydrology backward with Markov chain Monte Carlo simulation: FORCING DATA ERROR USING MCMC SAMPLING, *Water Resources Research*, 44(12), doi:10.1029/2007WR006720, 2008.

Vugrin, K. W., Swiler, L. P., Roberts, R. M., Stucky-Mack, N. J., and Sullivan, S. P.: Confidence region estimation techniques for nonlinear regression in groundwater flow: Three case studies, *Water Resour. Res.*, 43, W03423, doi:10.1029/2005WR004804, 2007.

Wiener, N.: The Homogeneous Chaos, *American Journal of Mathematics*, 60(4), 897, doi:10.2307/2371268, 1938.

Younes, A., Fahs, M. and Ahmed, S.: Solving density driven flow problems with efficient spatial discretizations and higher-order time integration methods, *Advances in Water Resources*, 32(3), 340–352, doi:10.1016/j.advwatres.2008.11.003, 2009.

Younes, A., Mara, T. A., Fajraoui, N., Lehmann, F., Belfort, B. and Beydoun, H.: Use of Global Sensitivity Analysis to Help Assess Unsaturated Soil Hydraulic Parameters, *Vadose Zone Journal*, 12(1), 0, doi:10.2136/vzj2011.0150, 2013.

Younes, A., Delay, F., Fajraoui, N., Fahs, M. and Mara, T. A.: Global sensitivity analysis and Bayesian parameter inference for solute transport in porous media colonized by biofilms, *Journal of Contaminant Hydrology*, 191, 1–18, doi:10.1016/j.jconhyd.2016.04.007, 2016.

Younes, A., Mara, T., Fahs, M., Grunberger, O. and Ackerer, P.: Hydraulic and transport parameter assessment using column infiltration experiments, *Hydrology and Earth System Sciences*, 21(5), 2263–2275, doi:10.5194/hess-21-2263-2017, 2017.

Zablocki, C.J.: Streaming potentials resulting from the descent of meteoric water: A possible source mechanism for Kilauean self-potential anomalies. *Trans. Geotherm. Resour. Council*. 2:747–748, 1978.



480 **List of table captions**

481 Table 1. Reference values, lower and upper bounds for hydraulic and geophysical parameters.

482 Table 2. The first-order sensitivity index S_i and the total sensitivity index ST_i for the SP
483 signal at 5 cm and 77 cm below the soil surface at different times.

484 Table 3: Estimated mean values (underlined), confidence intervals (CIs) and size of the
485 posterior CIs (italic) with MCMC and FOA approaches for scenario 1.

486 Table 4: Estimated mean values (underlined), confidence intervals (CIs) and size of the
487 posterior CIs (italic) with MCMC and FOA approaches for scenario 2.



Parameters	Lower bounds	Upper bounds	Reference values
K_s [cm min^{-1}]	0.1	2	0.495
θ_r [$\text{cm}^3 \text{min}^{-3}$]	0	0.2	0.045
α [cm^{-1}]	0.01	0.2	0.145
n	1.5	7	2.68
n_a [-]	1	3	1.6
$C_{sat} \times (-10^{-7})$ [V/Pa]	2	4	2.9

Table 1. Reference values, lower and upper bounds for hydraulic and geophysical parameters.

	K_s	θ_r	α	n	n_a	C_{sat}
a- sensor 1 (5 cm from the soil surface)						
t=10 min (total variance = 0.72)						
S_i	0.055	0	0	0	0	0.942
ST_i	0.057	0	0	0	0	0.945
t=70 min (total variance = 2.17)						
S_i	0.841	0.217	0.005	0.014	0.008	0.045
ST_i	0.894	0.043	0.008	0.028	0.021	0.078
t=800 min (total variance = 0.224)						
S_i	0.053	0.266	0.015	0.038	0.094	0.008
ST_i	0.085	0.738	0.065	0.266	0.472	0.041
b- sensor 4 (77 cm from the soil surface)						
t=10 min (total variance = 0.094)						
S_i	0.055	0	0	0	0	0.942
ST_i	0.057	0	0	0	0	0.945
t=70 min (total variance = 0.2744)						
S_i	0.839	0.015	0.014	0.013	0.005	0.053
ST_i	0.891	0.028	0.024	0.025	0.011	0.086
t=800 min (total variance = 0.224)						
S_i	0.099	0.225	0.054	0.043	0.085	0.01
ST_i	0.138	0.621	0.218	0.238	0.379	0.043

Table 2. The first-order sensitivity index S_i and the total sensitivity index ST_i for the SP

signal at 5 cm and 77 cm below the soil surface at different times.



	MCMC	FOA
K_s	<u>0.49</u> (0.487-0.498) <i>0.01</i>	<u>0.49</u> (0.487-0.497) <i>0.01</i>
θ_s	<u>0.43</u> (0.41-0.45) <i>0.04</i>	<u>0.43</u> (0.41-0.45) <i>0.04</i>
θ_r	<u>0.046</u> (0.025-0.068) <i>0.04</i>	<u>0.046</u> (0.026-0.066) <i>0.04</i>
α	<u>0.14</u> (0.12-0.17) <i>0.05</i>	<u>0.14</u> (0.12-0.16) <i>0.04</i>
n	<u>2.64</u> (2.54-2.77) <i>0.23</i>	<u>2.64</u> (2.54-2.76) <i>0.22</i>
n_a	<u>1.64</u> (1.37-1.98) <i>0.6</i>	<u>1.64</u> (1.38-1.90) <i>0.5</i>
C_{sat}	<u>2.90</u> (2.89-2.91) <i>0.02</i>	<u>2.90</u> (2.89-2.91) <i>0.02</i>

Table 3: Estimated mean values (underlined), confidence intervals (CIs) and size of the posterior CIs (italic) with MCMC and FOA approaches for scenario 1.



	MCMC	FOA
K_s	<u>0.49</u> (0.481-0.495) <i>0.014</i>	<u>0.49</u> (0.474-0.503) <i>0.029</i>
θ_s	<u>0.43</u> (0.41-0.45) <i>0.04</i>	<u>0.43</u> (0.41-0.45) <i>0.04</i>
θ_r	<u>0.053</u> (0.011-0.093) <i>0.08</i>	<u>0.053</u> (0.002-0.103) <i>0.1</i>
α	<u>0.13</u> (0.07-0.20) <i>0.13</i>	<u>0.13</u> (-0.15-0.43) <i>0.58</i>
n	<u>2.54</u> (2.44-2.68) <i>0.24</i>	<u>2.56</u> (2.44-2.68) <i>0.24</i>
n_a	<u>1.82</u> (1.36-2.41) <i>1.05</i>	<u>1.78</u> (1.29-2.27) <i>0.98</i>
C_{sat}	<u>2.89</u> (2.88-2.91) <i>0.03</i>	<u>2.89</u> (2.88-2.91) <i>0.03</i>

Table 4: Estimated mean values (underlined), confidence intervals (CIs) and size of the posterior CIs (italic) with MCMC and FOA approaches for scenario 2.



488

List of figure captions

489 Fig. 1. Reference SP signals. Solid lines represent the reference SP solution and dots represent
490 the sets of perturbed data serving as conditioning information for model calibration.

491

492 Figure 2. Time distribution of the SP variance at 5cm (a) and 77cm (b) depth. The shaded area
493 under the variance curve represents the partial marginal contributions of the random input
494 parameters; the contribution of interactions between parameters is represented by the blank
495 region between the shaded area and the variance curve.

496

497 Fig. 3: MCMC solutions when all SP data are considered for the calibration. The diagonal
498 plots represent the inferred posterior probability distribution of the model parameters. The
499 off-diagonal scatterplots represent the pairwise correlations in the MCMC drawing.

500

501 Fig. 4: MCMC solutions when calibration is performed using only SP data located at 5 cm
502 from the surface. The diagonal plots represent the posterior probability distribution of the
503 parameters. The off-diagonal scatterplots represent the pairwise correlations in the MCMC
504 drawing.

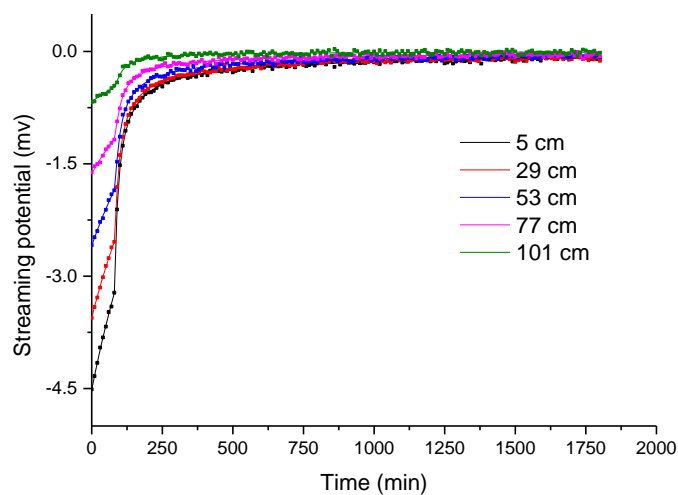


Fig. 1. Reference SP signals. Solid lines represent the reference SP solution and dots represent the sets of perturbed data serving as conditioning information for model calibration.

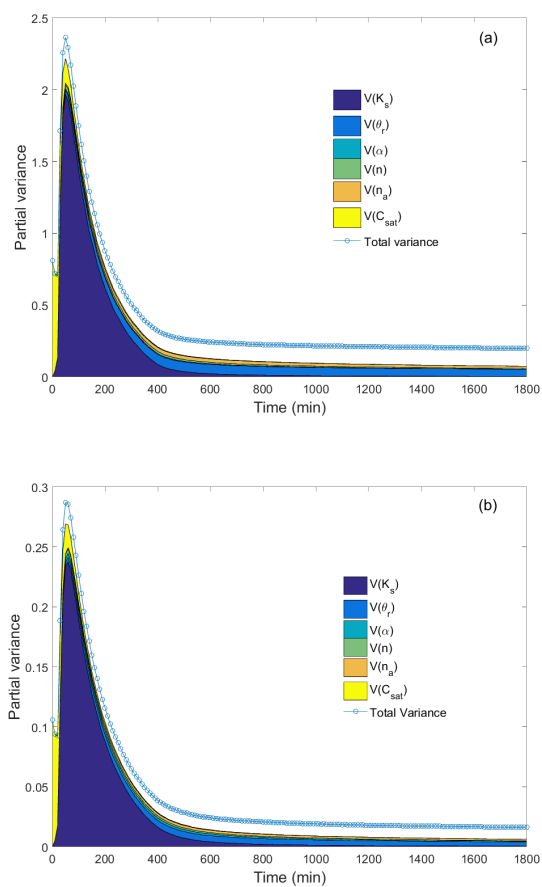


Figure 2. Time distribution of the SP variance at 5cm (a) and 77cm (b) depth. The shaded area under the variance curve represents the partial marginal contributions of the random input parameters; the contribution of interactions between parameters is represented by the blank region between the shaded area and the variance curve.

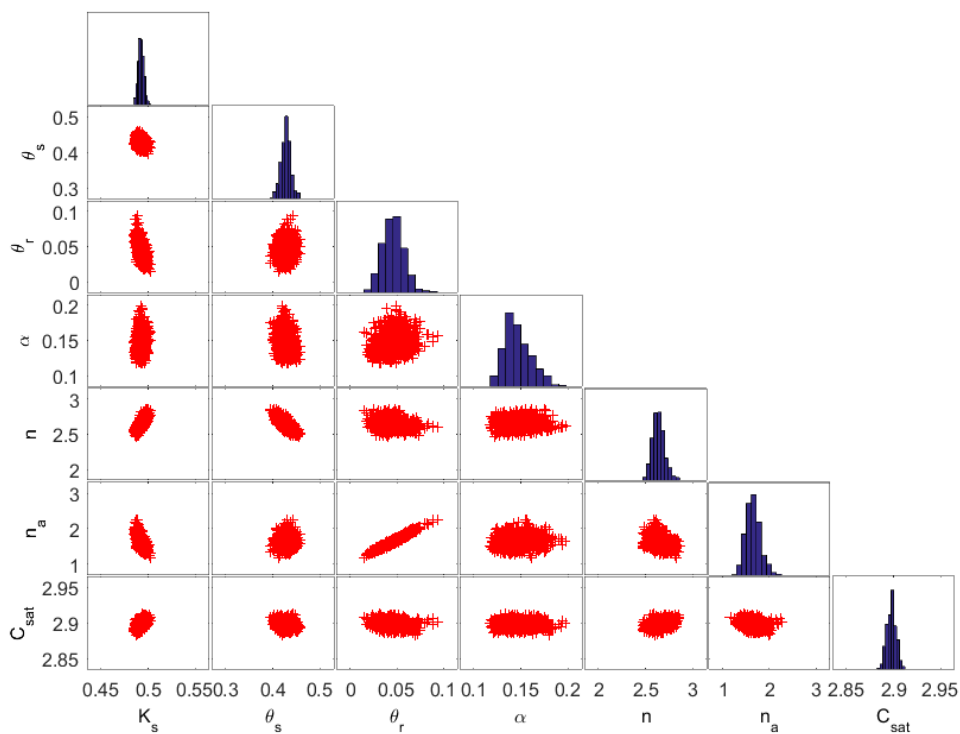


Fig. 3: MCMC solutions when all SP data are considered for the calibration. The diagonal plots represent the inferred posterior probability distribution of the model parameters. The off-diagonal scatterplots represent the pairwise correlations in the MCMC drawing.

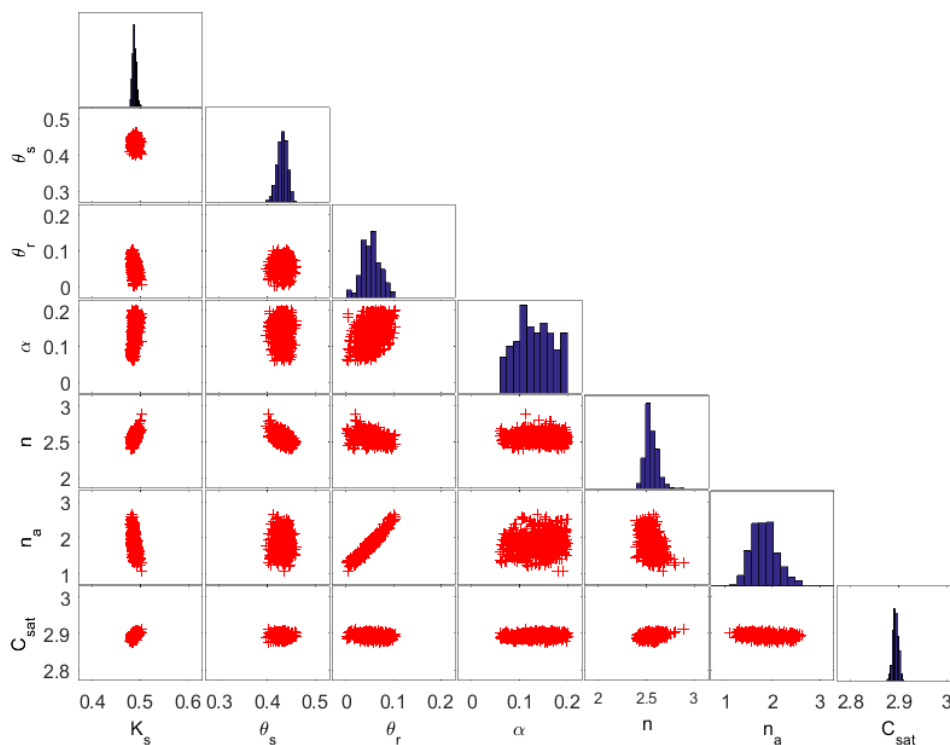


Fig. 4: MCMC solutions when calibration is performed using only SP data located at 5 cm from the surface. The diagonal plots represent the posterior probability distribution of the parameters. The off-diagonal scatterplots represent the pairwise correlations in the MCMC drawing.